Nanoscale Res Lett (2009) 4:1486–1492
DOI 10.1007/s11671-009-9425-4

NANO EXPRESS

# Hydrothermal Growth and Application of ZnO Nanowire Films with ZnO and $TiO_2$ Buffer Layers in Dye-Sensitized Solar Cells

**Weiguang Yang · Farong Wan · Siwei Chen · Chunhua Jiang**

Received: 26 April 2009 / Accepted: 18 August 2009 / Published online: 16 September 2009


**Abstract** This paper reports the effects of the seed layers prepared by spin-coating and dip-coating methods on the morphology and density of ZnO nanowire arrays, thus on the performance of ZnO nanowire-based dye-sensitized solar cells (DSSCs). The nanowire films with the thick ZnO buffer layer (~0.8–1 μm thick) can improve the open circuit voltage of the DSSCs through suppressing carrier recombination, however, and cause the decrease of dye loading absorbed on ZnO nanowires. In order to further investigate the effect of $TiO_2$ buffer layer on the performance of ZnO nanowire-based DSSCs, compared with the ZnO nanowire-based DSSCs without a compact $TiO_2$ buffer layer, the photovoltaic conversion efficiency and open circuit voltage of the ZnO DSSCs with the compact $TiO_2$ layer (~50 nm thick) were improved by 3.9–12.5 and 2.4–41.7%, respectively. This can be attributed to the introduction of the compact $TiO_2$ layer prepared by sputtering method, which effectively suppressed carrier recombination occurring across both the film–electrolyte interface and the substrate–electrolyte interface.

W. Yang · F. Wan (✉) · S. Chen
Department of Materials Physics and Chemistry, University of Science and Technology Beijing, 100083 Beijing, China
e-mail: wanfr@mater.ustb.edu.cn

W. Yang
e-mail: wgyangd@gmail.com

F. Wan
Beijing Key Lab of Advanced Energy Material and Technology, 100083 Beijing, China

C. Jiang
State Approved Technology Center, Irico Group Corp, 100085 Beijing, China

**Keywords** ZnO nanowires · Arrays · DSSC · Hydrothermal growth

## Introduction

Dye-sensitized solar cells (DSSCs) based on a dye-sensitized wide-band-gap nanocrystalline semiconductor (typically $TiO_2$) film have attracted widespread attention as a potential, cost-effective alternative to silicon solar cells since they were first introduced by O'Regan and Grätzel in 1991 [1]. As one of the key components of dye-sensitized solar cells, the photoelectrode, composed of nanocrystalline semiconductor materials accumulated on a transparent conducting glass, has a very important influence on the photovoltaic performance [2, 3]. It is well known that the energy conversion efficiency of DSSCs depends on the electron transport in the photoelectrode. Therefore, one-dimensional structure such as rods or wires of semiconductor materials can greatly improve DSSCs efficiency by offering direct electrical pathways for photogenerated electrons, thus enhancing the electron transport in the photoelectrode. Recently, considerable efforts have been devoted to the synthesis of such 1D materials used as the photoelectrodes of DSSCs [4–7].

Among various emerging 1D nanomaterials, ZnO, a wide-band-gap (3.37 eV) semiconductor with a large exciton binding energy of 60 meV at room temperature, is a promising alternative semiconductor to $TiO_2$. This is because that the band gap and the energetic position of the valence band maximum and conduction band minimum of ZnO are very close to that of $TiO_2$ and that the wurtzite structure of ZnO favors the formation of ordered 1D structures, moreover, presenting better electron transport compared with $TiO_2$ [4]. Consequently, the solar cell using

nanowire arrays as the photoelectrodes shows a higher conversion efficiency compared to those using the disorderedly structured ZnO films [4]. In order to further improve the cell efficiency, the effective approaches currently applied are to control the morphology of ZnO nanostructure films, which can significantly increase dye loading and light harvesting [8, 9], and to modify the surface of ZnO nanostructure films that can suppress carrier recombination [10]. However, by introducing a blocking layer at the base of the ZnO films, the influence of the blocking layer on the performance of ZnO DSSCs is an ongoing debate [10].

In this study, we report that the ZnO nanowire films with high aspect ratios and different thicknesses of ZnO buffer layers, which formed at the base of the nanowire films during growth, were prepared from different ZnO seed preparation methods. We also show that carrier recombination in ZnO nanowire-based dye-sensitized solar cells can be effectively suppressed and the photovoltaic conversion efficiency enhanced by introducing the $TiO_2$ buffer layer prepared by sputtering method.

## Experimental Section

### Materials

Polyethyleneimine (PEI, M.W.: 600) was purchased from Aldrich and used as received. *Cis*-bis (isothiocyanato) bis (2,2′-bipyridy1-4,4′-dicarboxylate) ruthenium (II) bistetrabutylammonium (also called N719) was from Solaronix SA, Switzerland. Other chemicals (Beijing Chemical Co.) used in our experiments were of analytical reagent grade without further purification. Fluorine-doped tin oxide substrates (FTO TEC-8, LOF) were first cleaned through sonication in acetone/ethanol for 30 min and then hydrolyzed in boiling deionized water at 100 °C for 30 min followed by air-drying.

### ZnO Nanowire Array Synthesis

ZnO nanowire arrays were made in aqueous solution, using a two-step process described elsewhere [4]. To study the effect of a thin compact $TiO_2$ film on FTO substrate on the solar cell performance of ZnO array film, it was prepared at room temperature by using reactive DC magnetron sputtering.

#### *Preparation of ZnO Seeds on FTO Substrates*

In order to study the effect of ZnO crystal seed particles on the morphology and solar cell performance of ZnO array film, they were coated onto the FTO substrates by using two different methods.

1. *Spin-coating method*. Zinc acetate dehydrate [$Zn(CH_3COO)_2{\cdot}2H_2O$] was dissolved in the mixed solution of ethanolamine and 2-methoxyethanol. The concentrations of both $Zn(CH_3COO)_2{\cdot}2H_2O$ and ethanolamine in the resulting solution are 0.75 M. The coating solution was spin-coated onto FTO substrates at 3,000 rpm for several times. The FTO substrates were subsequently annealed at 300 °C in air for 15 min in order to convert Zinc acetate to ZnO.
2. *Dip-coating method*. The FTO substrates were dip-coated in a 2.5 mM ethanolic solution of zinc acetate dehydrate. Following dip-coating, the zinc acetate films on the FTO substrates were annealed at 300 °C in air for 15 min.

#### *Hydrothermal Deposition*

ZnO nanowire arrays were grown by placing vertically the ZnO-seeded FTO substrates in solutions with 25 mM $Zn(NO_3)_2$, 25 mM hexamethylenetetramine (HMT) and 7.3 mM polyethyleneimine at 92.5 °C. In order to obtain a constant nanowire array growth rate, the solutions were refreshed during the reaction period (solution turnover time 2.5 h). Subsequently, the substrates were washed with water/ethanol and annealed at 400 °C for 30 min to remove any residual organics.

### Cell Assembly

The resulting substrates were immersed in dry ethanol containing 0.3 mM of N719 for 40 min. To assemble the solar cells, a Pt-coated conducting glass was placed on the ZnO nanowire array films separated by a 50-μm thin membrane spacer. The assembled cell was then clipped together as an open cell. An electrolyte, which was made with 0.1 M LiI (Aldrich), 0.1 M $I_2$ (Aldrich), 0.6 M dimethylpropylimidazolium iodide (DMPImI, Aldrich) and 0.5 M *tert*-butylpyridine (Aldrich) in dry acetonitrile (Aldrich), was injected into the open cell from the edges by capillarity.

### Characterization

The morphology of the products was characterized with use of field-emission scanning electron microscopy (FE-SEM, Hitachi S-4800). XRD analysis was performed on a powder X-ray diffractometer (Rigaku D/max-2500 diffractometer using CuK$\alpha$ radiation, $\lambda = 0.1542$, 40 kV, 100 mA). Photocurrent–voltage measurements were performed using simulated AM 1.5 sunlight with an output power of 100 mW $cm^{-2}$.

## Results and Discussion

### Effect of ZnO Crystal Seed Particles Prepared by Different Methods

In this study, we found that the different ZnO seed preparation methods strongly influenced the morphology and density of ZnO nanowire arrays, leading to the different performance of the DSSCs based on the ZnO nanowire films. Figure 1 shows the top-view and cross-sectional FESEM images of two samples prepared with 7.3 mM of PEI for 30 h on the FTO substrates with ZnO seed layers prepared by spin-coating and dip-coating. The mean values of the nanowire dimension, the array density and aspect ratio were estimated from a statistical evaluation of FE-SEM images and are summarized in Table 1. In order to avoid possible variations at their top, the diameters of the nanowires were measured slightly below the nanowire tip. Although they had the similar length, the diameter distributions between the well-aligned ZnO nanowires for samples A and B had a significant difference. The nanowire arrays for the samples A1, A2 and A3 had mean diameters ranging from 195 to 210 and 120 to 150 nm for samples B1, B2 and B3. The densities of ZnO nanowires for samples A1, A2 and A3 were 2.1, 2.2 and $2.0 \times 10^9$ wires $cm^{-2}$, respectively, which are much higher than that of samples B1, B2 and B3 ($1.5, 1.6, 1.2 \times 10^9$ wires $cm^{-2}$). The different thicknesses of ZnO buffer layers, which formed at the base of the nanowire films during growth, were obtained from different preparation ZnO seed methods: ~0.8–1 μm for samples A1, A2 and A3; ~300–500 nm for samples B1, B2 and B3. From the resulting observations, we can conclude that the high density of the nanowires achieved is attributed to the larger number of ZnO seeds on the FTO surface prepared by several spin-coating times [11, 12], and that, however, this seed preparation method results in a greater variation in nanowire diameter. The crystallinity of grown ZnO nanowire arrays on FTO substrate was investigated using X-ray diffraction. Because all the samples had the very similar XRD patterns, only the XRD pattern of sample B1 was shown in Fig. 2. Diffraction peaks in XRD pattern can be indexed as wurtzite hexagonal structure (JCPDS card No. 36-1451). With respect to the crystallographic orientation, the most

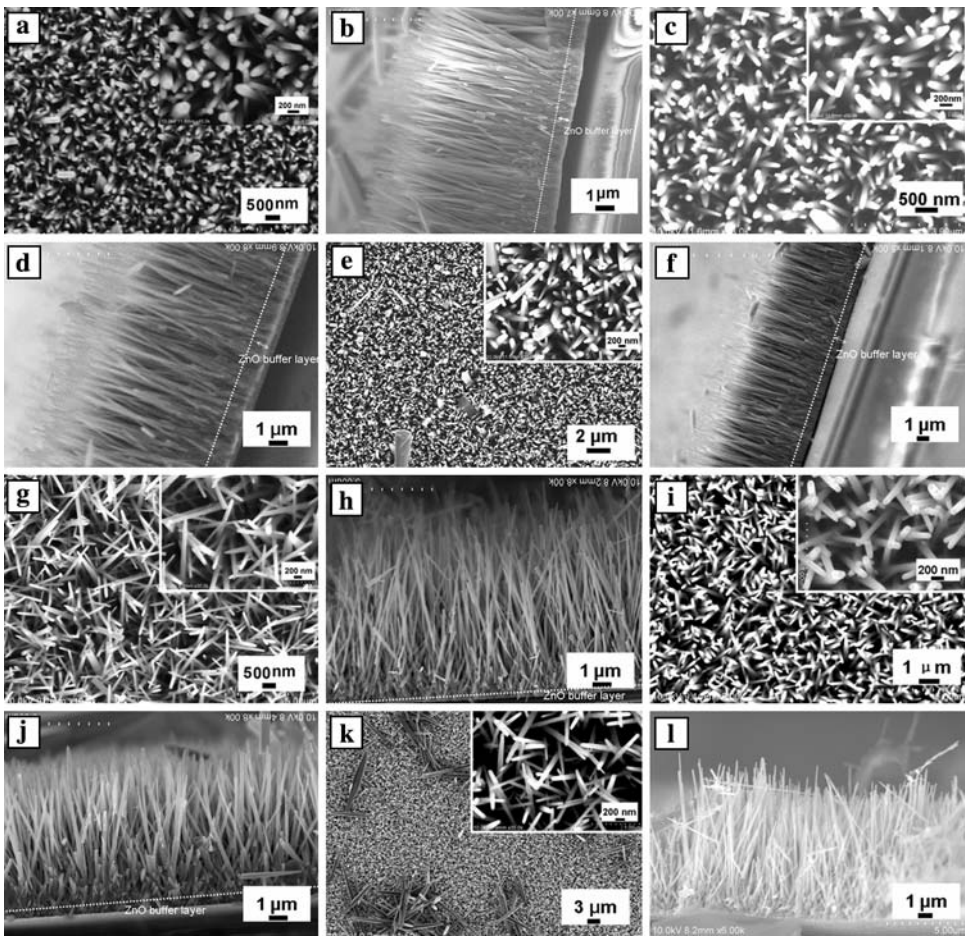


**Fig. 1** SEM images of ZnO nanowire arrays grown on FTO substrates with different ZnO seed obtained from (**a**–**f**) the spin-coating method, (**g**–**k**) the dip-coating method. **a**, **c**, **e**, **g**, **i** and **k** correspond to top-view observations, **b**, **d**, **f**, **h**, **j** and **l** correspond to cross-sectional views. The insets show high-magnification SEM images

**Table 1** Mean values of the nanowire dimensions, nanowire aspect ratio and array density for different ZnO seed preparation methods

| ZnO seed preparation methods | Diameter (nm) | Length (μm) | Nanowire aspect ratio | Density ($\times 10^9$ wires cm$^{-2}$) |
|---|---|---|---|---|
| Spin-coating | | | | |
| Sample A1 | 200 | 9.5 | 48 | 2.1 |
| Sample A2 | 195 | 9.1 | 47 | 2.2 |
| Sample A3 | 210 | 8.2 | 39 | 2.0 |
| Dip-coating | | | | |
| Sample B1 | 120 | 9.5 | 79 | 1.5 |
| Sample B2 | 150 | 8.2 | 55 | 1.6 |
| Sample B3 | 130 | 9.8 | 75 | 1.2 |

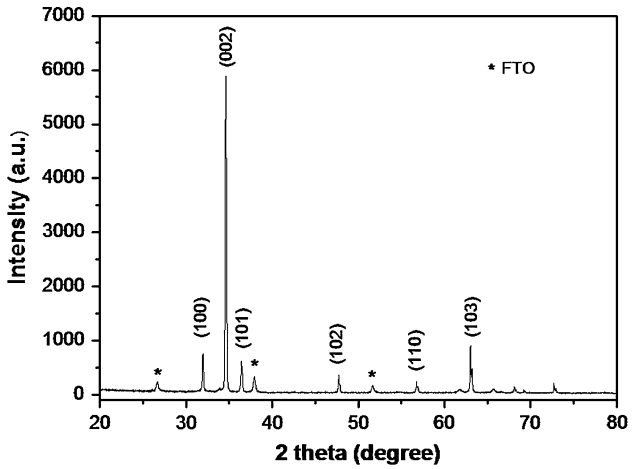


**Fig. 2** XRD pattern of the sample B1

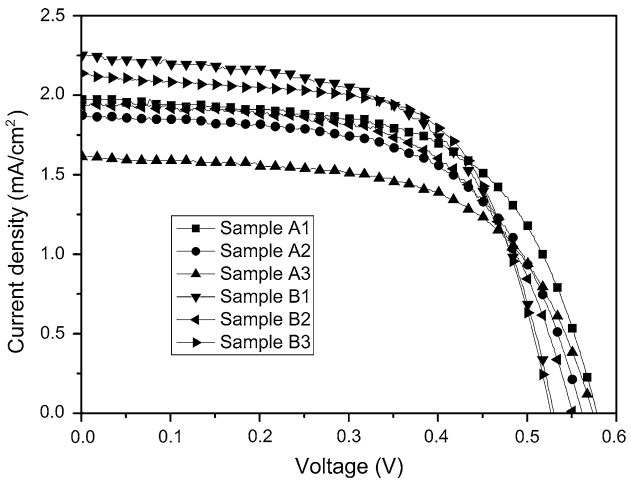


**Fig. 3** Current–voltage plots for ZnO DSSCs based on nanowire arrays prepared by different seed preparation methods

intense peak of ZnO corresponds to the (0002) plane, indicating a strong preferential orientation along the (0001) direction. The resulting observation can be inferred from SEM observations (Fig. 1b, d, f, h, j and l). These results reveal that the nanowires, crystallized along the ZnO (0001) direction, were hexagonal prisms vertically aligned on the FTO substrate.

The effect of the morphology and density of ZnO nanowire arrays on their DSSC performance was investigated, as shown in Fig. 3, while the parameters of dye-sensitized solar cell based on ZnO nanowire array films are listed in Table 2. Although the densities of nanowire arrays for samples B1, B2 and B3 were lower than that of samples A1, A2 and A3, the short circuit current density ($I_{sc}$) increased from 1.61–1.97 to 1.93–2.25 mA cm$^{-2}$, and in contrast, the open circuit voltage ($V_{oc}$) decreased from 0.57–0.58 to 0.54–0.56 V on using samples B1, B2 and B3 as the photoanode compared with samples A1, A2 and A3. The fill factor showed little change for all samples. The samples B1, B2 and B3 based DSSCs demonstrated higher energy conversion efficiency ($\eta$) of 0.66–0.73% when compared to the samples A1, A2 and A3 based DSSCs of 0.57–0.69%. The increase in $I_{sc}$ may be due to that the ZnO nanowires with the thin ZnO buffer layer (~300–500 nm) had higher aspect ratios (~55–79) compared with that (~39–48) of the ZnO nanowires with ~0.8–1 μm of the ZnO buffer layer, which caused the increase of dye loading absorbed on ZnO nanowires [13]. However, the ZnO buffer layer can act as a blocking layer to suppress carrier recombination that can occur across both the film–electrolyte interface and the substrate–electrolyte interface

**Table 2** Parameters of dye-sensitized solar cell based on ZnO nanowire array films with different ZnO seed preparation methods

| Sample | $I_{sc}$ (mA/cm$^2$) | Voc ($V$) | ff | $\eta$ (%) |
|---|---|---|---|---|
| Sample A1 | 1.97 | 0.58 | 0.60 | 0.69 |
| Sample A2 | 1.87 | 0.57 | 0.60 | 0.64 |
| Sample A3 | 1.61 | 0.58 | 0.61 | 0.57 |
| Sample B1 | 2.25 | 0.54 | 0.59 | 0.72 |
| Sample B2 | 1.93 | 0.56 | 0.61 | 0.66 |
| Sample B3 | 2.14 | 0.54 | 0.63 | 0.73 |

[10]. Therefore, the thin ZnO buffer layer can less effectively suppress carrier recombination than the thick ZnO buffer layer for sample A, resulting in the maximum loss of $V_{oc}$ (~40 mV).

## Effect of $TiO_2$ Blocking Layer

In this section, we investigated the influence of a dense, thin $TiO_2$ blocking layer (about 50 nm thick, as can be seen from Fig. 4h, j and l) underneath the ZnO nanowire array film prepared by sputtering method on carrier recombination in ZnO DSSC. Figure 4 shows the top-view and cross-sectional FESEM images of ZnO nanowire arrays prepared with 7.3 mM of PEI for 40 h on the bare FTO substrate and on the $TiO_2$-coated FTO substrate with the ZnO seeds prepared by dip-coating. The mean values of the nanowire dimension, the array density and aspect ratio are summarized in Table 3. As shown in Fig. 4, fairly well-aligned nanowires, typically 160–170 nm wide with the length of 10.6–11 μm, and 120–135 nm wide with the length of 10.8–11.2 μm, grew onto the bare and $TiO_2$-coated FTO substrates, respectively. The six ZnO nanowire films had a similar thickness of ZnO buffer layer (~500 nm). The density of ZnO nanowires for the bare FTO substrate were $1.4–1.6 \times 10^9$ wires $cm^{-2}$, which are slightly higher than that of the $TiO_2$-coated FTO substrate ($1.1–1.5 \times 10^9$ wires $cm^{-2}$).

The effect of the $TiO_2$ blocking layer on the photovoltaic performance of a DSSC was investigated. The current–voltage characteristics of the DSSCs for the bare and $TiO_2$-coated FTO substrates are shown in Fig. 5. The parameters of the cells are summarized in Table 4. The DSSC derived from the nanowire arrays with the $TiO_2$ blocking layer exhibited considerably improved $I_{sc}$ and $V_{oc}$, compared to that of the DSSC without the $TiO_2$ blocking layer. However, the change trend of the fill factor was complex. This is, $I_{sc}$ was increased by 4.2–25.1% from 3.31–3.77 to 3.72–4.14 mA $cm^{-2}$, and $V_{oc}$ was increased by 3.9–12.5% from 0.48–0.51 to 0.53–0.55 V. As a result, $\eta$ was improved by 2.4–41.7% from 0.72–0.84 to 0.86–1.02% by introducing the $TiO_2$ blocking layer. The increase in $I_{sc}$ can be attributed to the increase in the aspect ratio of the nanowire arrays with and without the $TiO_2$ blocking layer from about 65–67

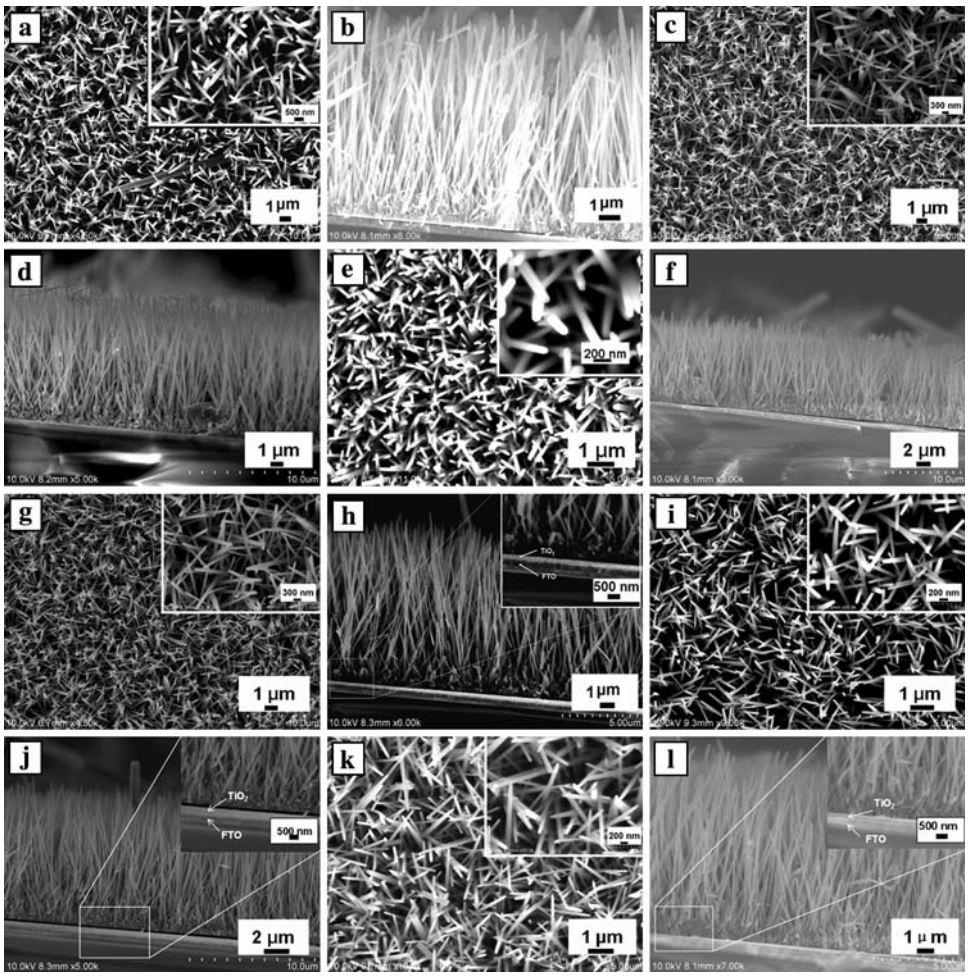


**Fig. 4** Top-view and cross-sectional SEM images of ZnO nanowire arrays prepared with 7.3 mM of PEI for 40 h **a**–**f** on the bare FTO substrate and **g**–**l** on the $TiO_2$-coated FTO substrate. The insets show high-magnification SEM images

**Table 3** Mean values of the nanowire dimensions, nanowire aspect ratio and array density for nanowire arrays on the bare and $TiO_2$-coated FTO substrates

| ZnO seed preparation methods | Diameter (nm) | Length (μm) | Nanowire aspect ratio | Density ($\times 10^9$ wires $cm^{-2}$) |
|---|---|---|---|---|
| Bare FTO substrates | | | | |
| Sample C1 | 170 | 11 | 65 | 1.4 |
| Sample C2 | 165 | 11 | 67 | 1.5 |
| Sample C3 | 160 | 10.6 | 66 | 1.6 |
| $TiO_2$-coated FTO | | | | |
| Sample D1 | 130 | 11 | 85 | 1.1 |
| Sample D2 | 120 | 11.2 | 93 | 1.2 |
| Sample D3 | 135 | 10.8 | 80 | 1.5 |

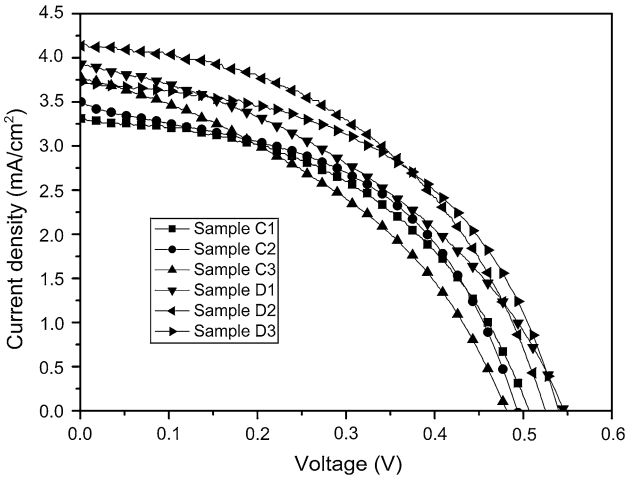


**Fig. 5** Current–voltage curves for ZnO DSSCs based on nanowire arrays grown onto the bare and $TiO_2$-coated FTO substrates

**Table 4** Parameters of dye-sensitized solar cell based on ZnO nanowire array films on the bare and $TiO_2$-coated FTO substrates

| Sample | $I_{sc}$ (mA/cm$^2$) | Voc ($V$) | ff | $\eta$ (%) |
|---|---|---|---|---|
| Sample C1 | 3.31 | 0.51 | 0.48 | 0.80 |
| Sample C2 | 3.50 | 0.49 | 0.49 | 0.84 |
| Sample C3 | 3.77 | 0.48 | 0.40 | 0.72 |
| Sample D1 | 3.93 | 0.55 | 0.40 | 0.86 |
| Sample D2 | 4.14 | 0.53 | 0.46 | 1.02 |
| Sample D3 | 3.72 | 0.54 | 0.50 | 1.01 |

to 80–93. $V_{oc}$ is known to be strongly dependent on the charge recombination reactions taking place on both the film–electrolyte interface and the substrate–electrolyte interface, a larger $V_{oc}$ value can be achieved through suppressing those reactions [14]. Therefore, the increase in $V_{oc}$ indicates that the compact $TiO_2$ layer prepared by sputtering method can effectively suppress the charge recombination. This clearly shows an effective increase in $\eta$ by introducing the $TiO_2$ blocking layer.

## Conclusion

In summary, the work presented here shows that the different ZnO seed preparation methods strongly influenced the morphology and density of ZnO nanowire arrays. The nanowire film growing from the ZnO seeds prepared by dip-coating had a thin ZnO buffer layer (~300–500 nm thick), which can less effectively suppress carrier recombination than the thick ZnO buffer layer (~0.8–1 μm thick) for spin-coating, resulting in the maximum loss of $V_{oc}$ (about 40 mV). In order to further investigate the effect of a $TiO_2$ buffer layer on the performance of ZnO nanowire-based DSSCs, a $TiO_2$ blocking layer (about 50 nm thick) underneath the ZnO nanowire array film was prepared onto the FTO substrate by sputtering method. The two different ZnO nanowire films with and without the compact $TiO_2$ buffer layer (~50 nm) had the similar thickness of ZnO buffer layer (~300–500 nm) and were used to assemble the DSSCs. By introducing the compact $TiO_2$ layer (~50 nm thick), the photovoltaic conversion efficiency and open circuit voltage of the ZnO DSSCs were improved by 3.9–12.5 and 2.4–41.7%, respectively. This can be because that the compact $TiO_2$ layer effectively suppressed carrier recombination occurring across both the film–electrolyte interface and the substrate–electrolyte interface.

**Acknowledgments** The authors would like to acknowledge financial support for this work from the Beijing Municipal Education Commission.

## References

1. B. O'Regan, M. Grätzel, Nature **353**, 737 (1991)
2. M.K. Nazeeruddin, P. Pechy, T. Renouard, S.M. Zakeeruddin, R. Humphry-Baker, P. Comte, P. Liska, L. Cevey, E. Costa, V. Shklover, L. Spiccia, G.B. Deacon, C.A. Bignozzi, M. Gratzel, J. Am. Chem. Soc. **123**, 1613 (2001)
3. C.D. Grant, A.M. Schwartzberg, G.P. Smestad, J. Kowalik, L. Tolbert, J.Z. Zhang, J. Electroanal. Chem. **522**, 40 (2002)
4. M. Law, L.E. Greene, J.C. Johnson, R. Saykally, P.D. Yang, Nat. Mater. **4**, 455 (2005)

5. S.H. Kang, S.-H. Chio, M.-S. Kang, J.-Y. Kim, H.-S. Kim, T. Hyeon, Y.-E. Sung, Adv. Mater. **20**, 54 (2008)
6. J.R. Jennings, A. Ghicov, L.M. Peter, P. Schmuki, A.B. Walker, J. Am. Chem. Soc. **130**, 13364 (2008)
7. M. Adachi, Y. Murata, J. Takao, J. Jiu, M. Sakamoto, F. Wang, J. Am. Chem. Soc. **126**, 14943 (2004)
8. Y. Gao, M. Nagai, T.-C. Chang, J.-J. Shyue, Cryst. Growth Des. **7**, 2467 (2007)
9. C.Y. Jiang, X.W. Sun, G.Q. Lo, D.L. Kwong, Appl. Phys. Lett. **90**, 263501 (2007)
10. M. Law, L.E. Greene, A. Radenovic, T. Kuykendall, J. Liphardt, P. Yang, J. Phys. Chem. B **110**, 22652 (2006)
11. S. Yamabi, H. Imai, J. Mater. Chem. **12**, 3773 (2002)
12. J. Elias, R. Tena-Zaera, C. Levy-Clement, Thin Solid Films **515**, 8553 (2007)
13. Y. Gao, M. Nagai, T.-C. Chang, J.-J. Shyue, Crys. Growth Des. **7**, 2467 (2007)
14. P.J. Cameron, L.M. Peter, J. Phys. Chem. B **107**, 14394 (2003)